ICC 2022 - IEEE International Conference on Communications | 978-1-5386-8347-7/22/$31.00 ©2022 IEEE | DOI: 10.1109/ICC45855.2022.9839119

Inter-Numerology Interference in 5G New Radio: Analysis and Bounds for Time-Varying Fading Channels

Tenneti Venkata Satya Sreedhar   Neelesh B. Mehta, *Fellow, IEEE*

***Abstract*—Mixed numerology is a new feature of the orthogonal frequency division multiplexing-based physical layer of 5G new radio (NR). It enables 5G to serve diverse use cases and services. However, the subcarriers of different numerologies, despite being non-overlapping in frequency, interfere with each other due to their different bandwidths and symbol durations. We derive novel expressions for the fading-averaged INI power at each subcarrier of a numerology in a wideband time-varying channel. These expressions cover the general family of numerologies of 5G NR, account for the guard band (which is used to mitigate INI), and apply to line-of-sight (LoS) and non-LoS channels. These lead to insightful expressions and tight bounds for the bandwidth-averaged INI power. They reveal that the INI power increases quadratically with the Doppler spread of the channel and affects higher-rate modulation and coding schemes.**

I. Introduction

Fifth generation (5G) wireless systems have been designed to provide unprecedented flexibility in supporting services with diverse requirements. In order to enable this, mixed numerology orthogonal frequency division multiplexing (OFDM) has been chosen as the physical layer [1]. The system bandwidth is divided into several non-overlapping bandwidth parts, and each bandwidth part can be assigned a different numerology.

Numerology specifies the subcarrier spacing, OFDM symbol duration, and cyclic prefix. The numerology chosen for a user depends upon the type of service and the frequency band of operation. For example, users with high mobility or stringent latency requirements use a larger subcarrier spacing. A larger spacing also counters the phase noise at higher carrier frequencies. On the other hand, a smaller subcarrier spacing is suitable for users operating in highly dispersive channels.

However, subcarriers with different bandwidths interfere with each other even though they are centered at different frequencies [2]. This leads to inter-numerology interference (INI) despite different physical resource blocks being assigned to different users. This new aspect of 5G OFDM systems causes an increase in the bit error rate (BER) and block error rate (BLER) and even error floors. The variation of the INI power across the subcarriers also affects the choice of subcarriers for reference signals [3]. While guard bands between the numerologies can be introduced to reduce the INI power, they reduce the spectral efficiency of the system.

A. Contributions and Comparison with Literature

In this paper, we develop a novel analysis of the INI powers encountered by mixed numerology systems in time-varying fading channels. We make the following contributions:

- We derive exact expressions for the fading-averaged INI power at each subcarrier in wideband fading channels. These general expressions apply to the family of numerologies adopted by 5G new radio (NR) in which the ratio of subcarrier bandwidths of the users is a power of two (e.g., 2, 4, 8, and 16). They account for the guard band, if present, and they apply to both line-of-sight (LoS) and non-LoS (NLoS) channels.
- We derive insightful expressions for the bandwidth-averaged INI power, which measures the INI power averaged across the subcarriers. Using these expressions, we derive novel and tight lower and upper bounds for the bandwidth-averaged INI power that show that it increases quadratically with the Doppler spread.
- Our numerical results using the tapped delay line (TDL) LoS and NLoS channel models specified in the 5G standard show that the INI due to numerologies with smaller or larger subcarrier spacings exhibits fundamentally different non-oscillatory and oscillatory behaviors. They reveal that the INI power is sufficiently large to affect the BLERs of modulation and coding schemes (MCSs) of 5G NR that use 64-QAM and 256-QAM [4, Table 5.1.3.1].

Literature and Comparisons: In [2], a spectrally efficient approach of allocating a guard band in mixed numerology systems is proposed. In [5], a resource allocation policy is proposed to minimize the inter-slice interference when network slicing is used. In [6], inter-slice/service-band-interference cancellation algrithms are proposed. In [7], closed-form expressions for INI are derived for a universal filtered multi-carrier based mixed numerology system for an additive white Gaussian noise (AWGN) channel. These expressions are used to determine the numerology and to allocate time-frequency resources to users in [8]. In [9], the power allocation and numerology are jointly selected for the uplink.

However, time-varying fading channels, which occur in many deployments, are not considered in [2], [5], [7]–[9].

T. V. S. Sreedhar is with the Central Research Laboratory at Bharat Electronics Limited, Bengaluru, India (email: sreedhartenneti@gmail.com).

Neelesh B. Mehta is with the Dept. of Electrical Communication Eng. at the Indian Institute of Science (IISc), Bengaluru, India (email: nbmehta@iisc.ac.in). This research was partially supported by the MEITY project "Next Generation Wireless Research and Standardization on 5G and Beyond."

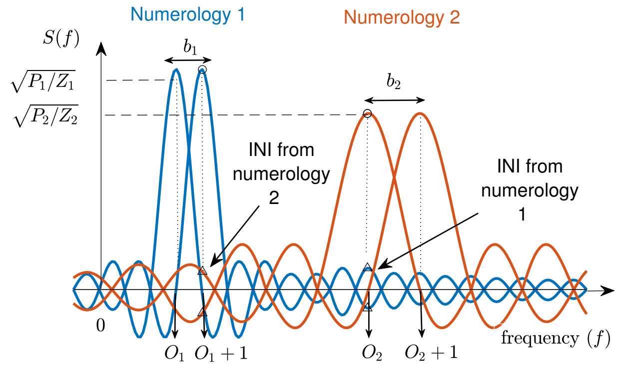

Fig. 1. Illustration of inter-numerology interference in a mixed numerology OFDM system ($b_2 = 2b_1$).

In [10], a block fading channel model is assumed, while in [3], a deterministic channel is assumed. These models do not capture the effect of Doppler spread. While [11] studies the factors that affect INI, it presents only simulation results for an AWGN channel.

B. Outline and Notation

The paper is organized as follows. In Section II, we present the system model. In Section III, we analyze INI in wideband time-varying fading channels. In Section IV, we derive bounds for the bandwidth-averaged INI power. Numerical results are presented in Section V. Our conclusions follow in Section VI.

Notation: The conjugate of a complex number z is denoted by z^*. Expectation is denoted by $\mathbb{E}[\cdot]$. We denote the sequence $X_0, X_1, \ldots, X_{K-1}$ by $\{X_k\}_{k=0}^{K-1}$.

II. System Model

Consider an OFDM downlink system with two users. User i is assigned a bandwidth part with numerology i. In the family of numerologies adopted in 5G NR, we have

$$b_2 = 2^{\mu} b_1 \text{ and } N_2^{\text{CP}} = N_1^{\text{CP}}/2^{\mu}, \tag{1}$$

where b_i and N_i^{CP} are the subcarrier spacing and cyclic prefix length, respectively, of numerology i, and μ is a positive integer. Without loss of generality, numerology 1 has a narrower subcarrier spacing. This analysis easily generalizes to the case of more than two users since the INI powers add up.

The n^{th} time-sample of the transmitted signal is given by

$$s(n) = \sqrt{P_1} s^{(1)}(n) + \sqrt{P_2} s^{(2)}(n), \tag{2}$$

where $s^{(i)}(n)$ is the signal for the user with numerology i, which has Z_i contiguous subcarriers and transmit power P_i.

For numerology i, $s^{(i)}(n)$ is given by

$$s^{(i)}(n) = \frac{1}{\sqrt{Z_i}} \sum_{u=0}^{Z_i-1} \sum_{v=-\infty}^{\infty} x_{u,v}^{(i)} g^{(i)}\left(n - vN_i^{\text{tot}}\right) \times \exp\left(j\frac{2\pi}{N_i}(u+O_i)\left(n - N_i^{\text{CP}} - vN_i^{\text{tot}}\right)\right), \tag{3}$$

where, for numerology i, $x_{u,v}^{(i)}$ is the symbol transmitted over subcarrier u of OFDM symbol v, N_i^{tot} is the OFDM symbol duration, and O_i is the frequency offset. Also, $\mathbb{E}\left[|x_{u,v}^{(i)}|^2\right] = 1$ and $N_i^{\text{tot}} = N_i + N_i^{\text{CP}}$, where N_i is the discrete Fourier transform (DFT) length. The transmit window $g^{(i)}(n)$ is 1, for $0 \le n < N_i^{\text{tot}}$, and is 0, otherwise.

The n^{th} time-sample of the received signal $y^{(i)}(n)$ of the user with numerology i is given by

$$y^{(i)}(n) = \sum_{l=0}^{L-1} h_l^{(i)}(n) s(n-l) + \omega^{(i)}(n), \tag{4}$$

where $\left\{h_l^{(i)}(n)\right\}_{l=0}^{L-1}$ are the time-domain channel taps of the user with numerology i. They are zero-mean, wide-sense stationary, and uncorrelated [13, Ch. 3]. And, $\omega^{(i)}(n)$ is AWGN noise with variance σ^2. The auto-correlation $r_l^{(i)}(w)$ of the l^{th} channel tap is defined as

$$r_l^{(i)}(w) \triangleq \mathbb{E}\left[h_l^{(i)}(n+w)\left(h_l^{(i)}(n)\right)^*\right]. \tag{5}$$

For example, for the classical Jakes' fading model, we have $r_l^{(i)}(w) = r_l^{(i)}(0) J_0(2\pi f_d w T_{\text{samp}})$, where $J_0(\cdot)$ is the zeroth-order Bessel function of the first kind, f_d is the Doppler spread, and T_{samp} is the sampling duration [14]. Without loss of generality, let $\sum_{l=0}^{L-1} r_l^{(i)}(0) = 1$. Note that both users' signals pass through the same channel for a given receiver.

Substituting (2) in (4), the expression for $y^{(i)}(n)$ becomes

$$y^{(i)}(n) = \sum_{l=0}^{L-1} h_l(n) s^{(1)}(n-l) + \sum_{l=0}^{L-1} h_l(n) s^{(2)}(n-l) + \omega^{(i)}(n). \tag{6}$$

For the receiver of the user with numerology i, the demodulated signal $\hat{y}_{k,m}^{(i)}$ at subcarrier k of OFDM symbol m is

$$\hat{y}_{k,m}^{(i)} = \frac{1}{\sqrt{N_i}} \sum_{n=-\infty}^{\infty} y^{(i)}(n) q^{(i)}\left(n - mN_i^{\text{tot}}\right) \times \exp\left(-j\frac{2\pi}{N_i}(k+O_i)\left(n - N_i^{\text{CP}} - mN_i^{\text{tot}}\right)\right), \tag{7}$$

where $q^{(i)}(n)$ is the rectangular receive window. It is 1, for $N_i^{\text{CP}} \le n < N_i^{\text{tot}}$, and is 0, otherwise.

From (7), it follows that the instantaneous INI $I_1^{\text{INI}}(k,m)$ at subcarrier k and OFDM symbol m at user 1's receiver due to numerology 2 is given by

$$I_1^{\text{INI}}(k,m) = \sqrt{\frac{P_2}{N_1}} \sum_{n=-\infty}^{\infty} \sum_{l=0}^{L-1} h_l^{(1)}(n) s^{(2)}(n-l) \times q^{(1)}\left(n - mN_1^{\text{tot}}\right) e^{-j\frac{2\pi}{N_1}(k+O_1)\left(n - N_1^{\text{CP}} - mN_1^{\text{tot}}\right)}. \tag{8}$$

Similarly, the INI $I_2^{\text{INI}}(k,m)$ at subcarrier k and OFDM symbol m at user 2's receiver due to numerology 1 equals

$$I_2^{\mathrm{INI}}(k,m) = \sqrt{\frac{P_1}{N_2}} \sum_{n=-\infty}^{\infty} \sum_{l=0}^{L-1} h_l^{(2)}(n)\, s^{(1)}(n-l) \times q^{(2)}\left(n - mN_2^{\mathrm{tot}}\right) e^{-j\frac{2\pi}{N_2}(k+O_2)\left(n-N_2^{\mathrm{CP}}-mN_2^{\mathrm{tot}}\right)}. \quad (9)$$

III. INI Analysis

We analyze the INI at the receivers of users 1 and 2 separately. Fig. 1 illustrates the INI at the two numerologies.

A. *INI at User* 1

Result *1:* The fading-averaged INI power $P_1^{\mathrm{INI}}(k)$ at subcarrier k of user 1's receiver due to numerology 2 equals

$$P_1^{\mathrm{INI}}(k) = \frac{P_2}{N_1 Z_2} \sum_{u=0}^{Z_2-1} \sum_{l=0}^{L-1} \left[\sum_{w=-(M-1+l)}^{M-1+l} r_l^{(1)}(w)\,(M+l-|w|) e^{-j\frac{2\pi\Delta_k^{(1)} w}{N_1}} + (2^\mu - 2) \sum_{w=-(N_2^{\mathrm{tot}}-1)}^{N_2^{\mathrm{tot}}-1} r_l^{(1)}(w)\left(N_2^{\mathrm{tot}} - |w|\right) e^{-j\frac{2\pi\Delta_k^{(1)} w}{N_1}} + \sum_{w=-\left(N_2^{\mathrm{tot}}-1-l\right)}^{N_2^{\mathrm{tot}}-1-l} r_l^{(1)}(w)\left(N_2^{\mathrm{tot}} - l - |w|\right) e^{-j\frac{2\pi\Delta_k^{(1)} w}{N_1}} \right], \quad (10)$$

where $M = N_2^{\mathrm{tot}} - N_1^{\mathrm{CP}}$ and $\Delta_k^{(1)} = k + O_1 - 2^\mu(u + O_2)$.

Proof: The proof is given in Appendix A. ■

$\Delta_k^{(1)}$ is the *spectral distance* between subcarrier k of numerology 1 and the interfering subcarrier u of numerology 2 [3]. It specifies how separated these two subcarriers are in multiples of numerology 1's subcarrier bandwidth.

B. *INI at User* 2

Result *2:* The fading-averaged INI power $P_2^{\mathrm{INI}}(k)$ at subcarrier k of user 2's receiver due to numerology 1 equals

$$P_2^{\mathrm{INI}}(k) = \frac{P_1}{N_2 Z_1} \sum_{u=0}^{Z_1-1} \sum_{l=0}^{L-1} \sum_{w=-(N_2-1)}^{N_2-1} r_l^{(2)}(w) \times (N_2 - |w|)\, e^{-j\frac{2\pi}{N_1}\Delta_k^{(2)} w}, \quad (11)$$

where $\Delta_k^{(2)} = 2^\mu(k+O_2) - (u+O_1)$ is the spectral distance between the victim subcarrier k of numerology 2 and the interfering subcarrier u of numerology 1.

Proof: The proof is similar to Appendix A, and is skipped. ■

The above results apply to LoS and NLoS fading channels, for which the expressions for $r_0^{(i)}(w)$ are different.

IV. Insights: Bandwidth-Averaged INI Power and Bounds

To gain further insights, we analyze the band-width averaged INI power $\overline{P}_1^{\mathrm{INI}}$, which is defined as $\overline{P}_1^{\mathrm{INI}} = \left(\sum_{k=0}^{Z_1-1} P_1^{\mathrm{INI}}(k)\right)/Z_1$. Intuitively, the larger this value, the more is the INI. We focus on the scenario where the two numerologies together occupy the entire bandwidth, i.e., $Z_2 + (Z_1/2^\mu) = N_2$, $O_1 = 0$, and there is no guard band, i.e., $O_2 = Z_1/2^\mu$. The expressions and bounds for $\mu \geq 2$ can be obtained in a similar manner. They are lengthier and are not shown to conserve space.

As shown in Appendix B,

$$\overline{P}_1^{\mathrm{INI}} = \frac{P_2}{N_1 Z_1 Z_2} \left[N_1 Z_1 Z_2 - 2\sum_{l=0}^{L-1} \sum_{w=1}^{M-1+l} r_l^{(1)}(w)\,(M+l-w)\,\phi_1(w,\mu) - 2\left(2^\mu - 2\right) \sum_{l=0}^{L-1} \sum_{w=1}^{N_2^{\mathrm{tot}}-1} r_l^{(1)}(w)\left(N_2^{\mathrm{tot}} - w\right)\phi_1(w,\mu) - 2\sum_{l=0}^{L-1} \sum_{w=1}^{N_2^{\mathrm{tot}}-1-l} r_l^{(1)}(w)\left(N_2^{\mathrm{tot}} - l - w\right)\phi_1(w,\mu) \right], \quad (12)$$

where the function $\phi_i(.,.)$ is defined as

$$\phi_i(w,\mu) \triangleq \frac{\cos\left(\frac{\pi w(2^\mu - 1)}{N_i}\right)\left[\sin\left(\frac{\pi Z_i w}{N_i}\right)\right]^2}{\sin\left(\frac{\pi w}{N_i}\right)\sin\left(\frac{\pi 2^\mu w}{N_i}\right)}. \quad (13)$$

We now bound $\overline{P}_1^{\mathrm{INI}}$. Let $\alpha_1 \triangleq \int_{-f_d}^{f_d}\left(\frac{f}{f_d}\right)^2 S(f)\,df$ and $\alpha_2 \triangleq \int_{-f_d}^{f_d}\left(\frac{f}{f_d}\right)^4 S(f)\,df$ denote the normalized second and fourth moments, respectively, of the Doppler spectrum $S(f)$ [15]. For example, for the Jakes' fading model, $\alpha_1 = 1/2$ and $\alpha_2 = 3/8$.

Result *3:* The bandwidth-averaged INI power $\overline{P}_1^{\mathrm{INI}}$ at user 1 is upper and lower bounded as follows:

$$\overline{P}_1^{\mathrm{INI}} \leq \frac{P_2}{N_1 Z_1 Z_2} \sum_{l=0}^{L-1} r_l^{(1)}(0) \left[N_1 Z_1 Z_2 - \psi_1(0, M+l) - \psi_1\left(0, N_2^{\mathrm{tot}} - l\right) + \frac{\alpha_1}{2}\left[\psi_1(2, M+l) + \psi_1\left(2, N_2^{\mathrm{tot}} - l\right)\right]\left(\frac{2\pi f_d T_s^{(1)}}{N_1}\right)^2 \right], \quad (14)$$

$$\overline{P}_1^{\mathrm{INI}} \geq \frac{P_2}{N_1 Z_1 Z_2} \sum_{l=0}^{L-1} r_l^{(1)}(0) \left[N_1 Z_1 Z_2 - \psi_1(0, M+l) - \psi_1\left(0, N_2^{\mathrm{tot}} - l\right) + \frac{\alpha_1}{2}\left[\psi_1(2, M+l) + \psi_1\left(2, N_2^{\mathrm{tot}} - l\right)\right]\left(\frac{2\pi f_d T_s^{(1)}}{N_1}\right)^2 - \frac{\alpha_2}{24}\left[\psi_1(4, M+l) + \psi_1\left(4, N_2^{\mathrm{tot}} - l\right)\right]\left(\frac{2\pi f_d T_s^{(1)}}{N_1}\right)^4 \right], \quad (15)$$

where the function $\psi_i(.,.)$ is defined as

$$\psi_i(p,q) \triangleq \sum_{w=1}^{q-1} w^p (q-w) \left(\frac{\sin(\pi w Z_i / N_i)}{\sin(\pi w / N_i)} \right)^2 . \tag{16}$$

Proof: The proof is given in Appendix C. ■

Similarly, from Result 2, we can show that the bandwidth-averaged INI power $\overline{P}_2^{\mathrm{INI}}$ at user 2, which is defined as $\overline{P}_2^{\mathrm{INI}} = \left(\sum_{k=0}^{Z_2-1} P_2^{\mathrm{INI}}(k) \right) / Z_2$, is given by

$$\overline{P}_2^{\mathrm{INI}} = \frac{P_1}{N_2 Z_1 Z_2} \Big[N_2 Z_1 Z_2 - 2 \sum_{l=0}^{L-1} \sum_{w=1}^{N_2-1} r_l^{(2)}(w) (N_2 - w) \phi_1(w,\mu) \Big] . \tag{17}$$

As above, we can prove that $\overline{P}_2^{\mathrm{INI}}$ is upper and lower bounded as follows:

$$\overline{P}_2^{\mathrm{INI}} \leq \frac{P_1}{N_2 Z_1 Z_2} \left[N_2 Z_1 Z_2 - \psi_1(0, N_2) + \frac{\alpha_1}{2} \psi_1(2, N_2) \left(\frac{2\pi f_d T_s^{(1)}}{N_1} \right)^2 \right], \tag{18}$$

$$\overline{P}_2^{\mathrm{INI}} \geq \frac{P_1}{N_2 Z_1 Z_2} \left[N_2 Z_1 Z_2 + \frac{\alpha_1}{2} \psi_1(2, N_2) \left(\frac{2\pi f_d T_s^{(1)}}{N_1} \right)^2 - \psi_1(0, N_2) - \frac{\alpha_2}{24} \psi_1(4, N_2) \left(\frac{2\pi f_d T_s^{(1)}}{N_1} \right)^4 \right]. \tag{19}$$

Comments: Equations (12) and (17) bring out the dependence of the bandwidth-averaged INI powers on the number of subcarriers, transmit powers, and spectral distances of the two numerologies and the auto-correlation of the channel.

The effect of the Doppler spectrum is captured by the two moments α_1 and α_2. The quadratic term $\left(f_d T_s^{(1)} \right)^2$ is dominant in the bounds for both users. While it is $\alpha_1 \left[\psi_1(2, M+l) + \psi_1(2, N_2^{\mathrm{tot}} - l) \right]/2$ for user 1, it is $\alpha_1 \psi_1(2, N_2)/2$ for user 2. Another difference is that the bounds in (18) and (19) for the bandwidth-averaged INI power at user 2 do not depend on the powers of the channel taps $r_0^{(2)}(0), r_1^{(2)}(0), \ldots, r_{L-1}^{(2)}(0)$. However, this is not the case for user 1. This can be understood as follows. The second argument of the $\psi_1(.,.)$ is the overlap between the receive window of the victim numerology and the channel-delayed transmit window of the interfering numerology. For user 2's receiver, this overlapping window length is the same for all paths. On the other hand, for user 1's receiver, the overlapping window length is a function of the path delay.

V. Numerical Results

We use the following parameters in our Monte Carlo simulations. For numerology 1, the subcarrier spacing is 15 kHz, OFDM symbol duration is 66.67 μs, and DFT size is 512. For numerology 2, we use multiple sets of parameters to understand its impact; these are mentioned in the figure descriptions. The sampling rate is 7.68 MHz for all the numerologies. We use the TDL-C and TDL-D models that are specified in 5G NR for NLoS and LoS channels, respectively [16]. The delay spread is 100 ns and $f_d = 30$ Hz. The simulation results are averaged over 1000 independent channel realizations.

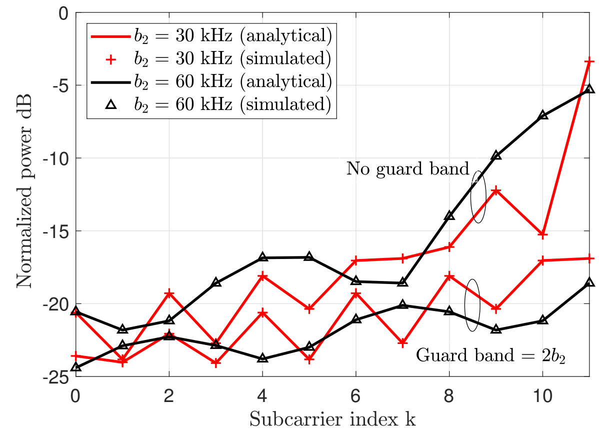

Fig. 2. Normalized fading-averaged INI power at each subcarrier of user 1, $P_1^{\mathrm{INI}}(k)/(P_1/Z_1)$, in TDL-D LoS channel ($P_2 = P_1$, $Z_1 = 12$, $Z_2 = 12$, $O_1 = 60$, $O_2 = 36$, $T_s^{(1)} = 66.67$ μs, $N_2 = 256$ when $b_2 = 30$ kHz, and $N_2 = 128$ when $b_2 = 60$ kHz).

Fig. 2 plots the fading-averaged INI power normalized with respect to the power per subcarrier, i.e., $P_1^{\mathrm{INI}}(k)/(P_1/Z_1)$, at each subcarrier of user 1. The results are generated for the TDL-D LoS channel for two subcarrier bandwidths of numerology 2, and with and without a guard band. The analytical and simulation results match well. The INI power exhibits an oscillatory behavior. Subcarriers closer to the interfering numerology experience more INI compared to those that are farther. Increasing the guard band reduces the INI power on each subcarrier of numerology 1. When the subcarrier spacing of numerology 2 is 30 kHz and there is no guard band, the normalized fading-averaged INI power varies from -4 to -24 dB. Thus, the INI power exhibits a wide dynamic range of 20 dB across the subcarriers.

Fig. 3 shows the corresponding results for the fading-averaged INI power at each subcarrier of user 2. The INI power at user 2 also has a large dynamic range of 21.7 dB. Unlike Fig. 2, the INI power at user 2 monotonically decreases as the subcarrier index increases. The oscillatory behavior in Fig. 2 can be understood from (10), which has the form of a discrete Fourier transform of a decreasing ramp function that is evaluated at the spectral distance $\Delta_k^{(1)}$. This is oscillatory in nature. While (11) also has a similar form, it is evaluated at the spectral distance $\Delta_k^{(2)}$, which is larger by a factor 2^{μ}.

Fig. 4 plots the bandwidth-averaged INI power at user 1, which is given in (12), as a function of the scaled Doppler spread $f_d T_s^{(i)}$. The INI power is normalized with respect to the transmit power per subcarrier of the user's numerology. It is plotted in linear scale in order to easily see its dependence

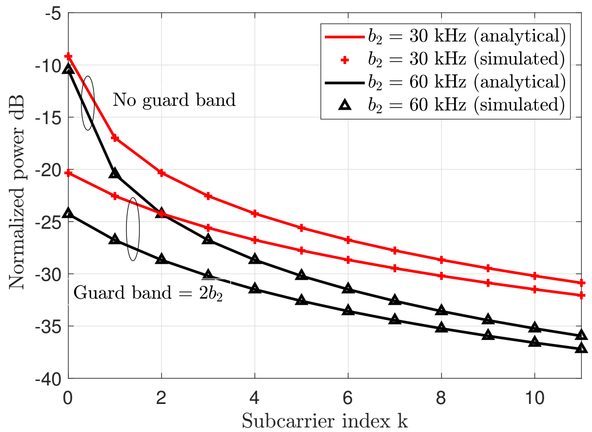

Fig. 3. Normalized fading-averaged INI power at each subcarrier of user 2, $P_2^{\text{INI}}(k)/(P_2/Z_2)$, in TDL-D LoS channel ($P_2 = P_1$, $Z_1 = 12$, $Z_2 = 12$, $O_1 = 60$, $O_2 = 36$, and $T_s^{(1)} = 66.67\ \mu$s, $N_2 = 256$ when $b_2 = 30$ kHz, and $N_2 = 128$ when $b_2 = 60$ kHz).

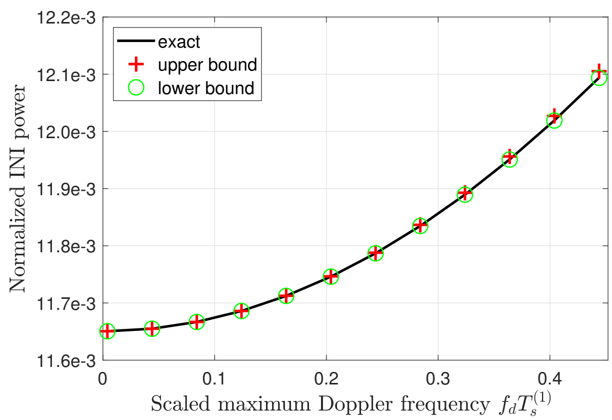

Fig. 4. Normalized bandwidth-averaged INI power, $\overline{P}_1^{\text{INI}}/(P_1/Z_1)$, and bounds for user 1 in the TDL-C NLoS channel. Results are shown in linear scale ($P_2 = 2P_1$, $Z_1 = 256$, $T_s^{(1)} = 66.67\ \mu$s, $Z_2 = 128$, $N_2 = 256$, no guard band, and $b_2 = 30$ kHz).

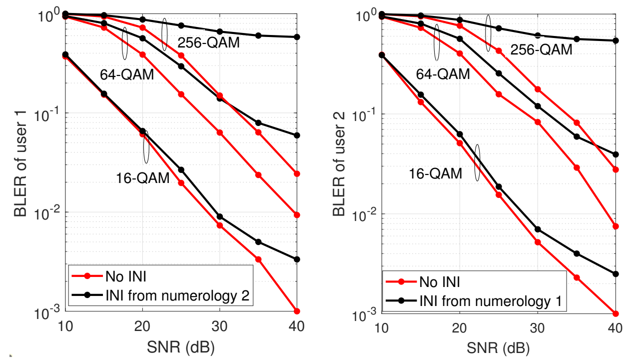

(a) On user 1 ($P_2 = 5P_1$) (b) On user 2 ($P_1 = 7P_2$)

Fig. 5. Degradation of BLER due to INI of users 1 and 2 for different MCSs of 5G NR in TDL-C NLoS channel ($Z_1 = 12$, $Z_2 = 84$, $O_1 = 6$, $O_2 = 172$, $N_2 = 256$, $b_2 = 30$ kHz, and 90 kHzguard band).

on f_d. Also shown are the bounds. We see that the bounds are tight, which shows the efficacy of the bounding approach, and the bandwidth-averaged INI power scales quadratically with f_d. The INI power is non-zero even for $f_d = 0$ Hz. It takes a value of $11.65 \times 10^{-3}(-19.3$ dB), which is significant for higher order MCSs that require signal-to-noise-ratios (SNRs) greater than 22.25 dB for successful decoding. The same trend is observed in the case of user 2, whose figure is not shown.

Impact of INI: Fig. 5 studies the impact of INI at each user for different MCSs specified in 5G NR and for different values of P_1 and P_2. For this, it plots the BLER, which is the metric used to evaluate performance of a block of coded data that is transmitted in a cellular system, as a function of the SNR. The BLER curves are generated using the 5G toolbox of Matlab as follows. The 5G physical layer compliant mixed numerology signal containing transport blocks of both numerologies is generated and transmitted through a realization of the TDL-C channel. The AWGN noise is added at each user's receiver. The corresponding decoding blocks for each user's receiver are implemented. In the computation of the log-likelihood ratios, which are passed to the low-density parity check decoder to decode the transport block, the instantaneous INI powers at the subcarriers of both the users, computed using [3, (57)], are used. We show results for MCSs 16 and 28, which use 16-QAM and 64-QAM modulations, respectively [4, Table 5.1.3.1-1], and MCS 27, which uses 256-QAM modulation [4, Table 5.1.3.1-2]. The results are shown with and without INI. We see that INI causes a significant degradation of BLER for the higher rate MCSs that use 64-QAM and 256-QAM.

VI. Conclusions

We derived closed-form expressions for the fading-averaged and bandwidth-averaged INI powers in the downlink of mixed numerology OFDM systems that are employed by 5G NR. The INI powers exhibited a wide dynamic range across the subcarriers. The INI power at the numerology with narrower subcarrier bandwidths showed an oscillatory behavior while that at the other numerology did not. The INI powers of the subcarriers closer to the interfering numerology were larger than for the central subcarriers. We also derived novel and insightful expressions and lower and upper bounds for the bandwidth-averaged INI power, which brought out its quadratic dependence on the Doppler spread. Our analysis showed that the INI power was sufficiently large to affect the BLERs of the higher rate MCSs of 5G NR and necessity of INI mitigation techniques.

Appendix

A. Proof of Result 1

The transmit symbols $\left\{x^{(2)}_{u,2^\mu m}\right\}_{u=0}^{Z_2-1}$, $\left\{x^{(2)}_{u,2^\mu m+1}\right\}_{u=0}^{Z_2-1}, \ldots, \left\{x^{(2)}_{u,2^\mu (m+1)-1}\right\}_{u=0}^{Z_2-1}$ are independent and identically distributed with zero-mean and unit variance, and the channel taps are uncorrelated. Therefore, from (8), we get

$$P_1^{\text{INI}}(k) = \mathbb{E}\left[\left|I_1^{\text{INI}}(k,m)\right|^2\right] = \frac{P_2}{N_1 Z_2}\sum_{l=0}^{L-1}\sum_{u=0}^{Z_2-1}$$

$$\left(\mathbb{E}\left[\left|\sum_{n'=0}^{M-1+l} h_l\left(n' + N_1^{\text{CP}} + mN_1^{\text{tot}}\right) e^{-\frac{j2\pi}{N_1}\Delta_k^{(1)} n'}\right|^2\right]\right.$$

$$+ (2^\mu - 2)\,\mathbb{E}\left[\left|\sum_{n'=0}^{N_2^{\text{tot}}-1} h_l\left(n' + N_1^{\text{CP}} + mN_1^{\text{tot}}\right) e^{-\frac{j2\pi}{N_1}\Delta_k^{(1)} n'}\right|^2\right]$$

$$\left.+\mathbb{E}\left[\left|\sum_{n'=M+l}^{N_1-1} h_l\left(n' + N_1^{\text{CP}} + mN_1^{\text{tot}}\right) e^{-\frac{j2\pi}{N_1}\Delta_k^{(1)} n'}\right|^2\right]\right). \tag{20}$$

Using the definition of auto-correlation in (5), we get

$$P_1^{\text{INI}}(k) = \frac{P_2}{N_1 Z_2}\sum_{u=0}^{Z_2-1}\sum_{l=0}^{L-1}$$

$$\left[\sum_{s=0}^{M-1+l}\sum_{t=0}^{M-1+l} r_l^{(1)}(s-t)\, e^{-j\frac{2\pi}{N_1}\Delta_k^{(1)}(s-t)}\right.$$

$$+ (2^\mu - 2)\sum_{s=0}^{N_2^{\text{tot}}-1}\sum_{t=0}^{N_2^{\text{tot}}-1} r_l^{(1)}(s-t)\, e^{-j\frac{2\pi}{N_1}\Delta_k^{(1)}(s-t)}$$

$$\left.+\sum_{s=0}^{N_2^{\text{tot}}-1-l}\sum_{t=0}^{N_2^{\text{tot}}-1-l} r_l^{(1)}(s-t)\, e^{-j\frac{2\pi}{N_1}\Delta_k^{(1)}(s-t)}\right]. \tag{21}$$

Using the transformation $s - t = w$ yields the result in (10).

B. Derivation of (12)

From (10), the bandwidth-averaged INI power $\overline{P}_1^{\text{INI}}$ at user 1 is given by

$$\overline{P}_1^{\text{INI}} = \frac{P_2}{N_1 Z_2 Z_1}\sum_{k=0}^{Z_1-1}\sum_{u=0}^{Z_2-1}\sum_{l=0}^{L-1}$$

$$\left[\sum_{w=-(M-1+l)}^{M-1+l} r_l^{(1)}(w)\,(M+l-|w|)e^{\frac{-j2\pi\Delta_k^{(1)}w}{N_1}}\right.$$

$$+ (2^\mu - 2)\sum_{w=-(N_2^{\text{tot}}-1)}^{N_2^{\text{tot}}-1} r_l^{(1)}(w)\,(N_2^{\text{tot}}-|w|)e^{\frac{-j2\pi\Delta_k^{(1)}w}{N_1}}$$

$$\left.+\sum_{w=-(N_2^{\text{tot}}-1-l)}^{N_2^{\text{tot}}-1-l} r_l^{(1)}(w)\,(N_2^{\text{tot}}-l-|w|)e^{\frac{-j2\pi\Delta_k^{(1)}w}{N_1}}\right]. \tag{22}$$

The innermost summation in (22) can be simplified using the following identity, whose proof we skip:

$$\sum_{k=0}^{Z_1-1}\sum_{u=0}^{Z_2-1}\sum_{w=-(K-1)}^{K-1} r_l^{(1)}(w)\,(K-|w|)\, e^{\frac{-j2\pi\left(k-2^\mu u - Z_1\right)w}{N_1}}$$

$$= KZ_1Z_2 r_l^{(1)}(0) - 2\sum_{w=1}^{K-1} r_l^{(1)}(w)\,(K-w)\,\phi_1(w,\mu). \tag{23}$$

It holds when Z_1 and Z_2 are even. Substituting this and $N_1 = M + N_2^{\text{tot}}$ in (22) yields (12).

C. Proof of Result 3

The proof is based on the following two inequalities for the auto-correlation $r_l^{(i)}(w)$ of the l^{th} channel tap [15, Sec. III-B]:

$$r_l^{(i)}(w) \geq r_l^{(i)}(0)\left[1 - \frac{\alpha_1}{2}\left(\frac{2\pi f_d w T_s^{(i)}}{N_i}\right)^2\right], \tag{24}$$

$$r_l^{(i)}(w) \leq r_l^{(i)}(0)\left[1 - \frac{\alpha_1}{2}\left(\frac{2\pi f_d w T_s^{(i)}}{N_i}\right)^2 + \frac{\alpha_2}{24}\left(\frac{2\pi f_d w T_s^{(i)}}{N_i}\right)^4\right]. \tag{25}$$

Substituting the above bounds in (12) and (17), and simplifying much further yields the bounds for $\overline{P}_1^{\text{INI}}$ and $\overline{P}_2^{\text{INI}}$.

REFERENCES

[1] A. A. Zaidi, R. Baldemair, H. Tullberg, H. Bjorkegren, L. Sundstrom, J. Medbo, C. Kilinc, and I. Da Silva, "Waveform and numerology to support 5G services and requirements," *IEEE Commun. Mag.*, vol. 54, no. 11, pp. 90–98, Nov. 2016.

[2] E. Memisoglu, A. B. Kihero, E. Basar, and H. Arslan, "Guard band reduction for 5G and beyond multiple numerologies," *IEEE Commun. Lett.*, vol. 24, no. 3, pp. 644–647, Mar. 2020.

[3] X. Zhang, L. Zhang, P. Xiao, D. Ma, J. Wei, and Y. Xin, "Mixed numerologies interference analysis and inter-numerology interference cancellation for windowed OFDM systems," *IEEE Trans. Veh. Technol.*, vol. 67, no. 8, pp. 7047–7061, Aug. 2018.

[4] "Physical layer procedures for data (release 15)," 3rd Generation Partnership Project (3GPP), Tech. Rep. 38.214 (v15.3.0), 2018.

[5] M. Zambianco and G. Verticale, "Interference minimization in 5G physical-layer network slicing," *IEEE Trans. Commun.*, vol. 68, no. 7, pp. 4554–4564, Mar. 2020.

[6] B. Yang, L. Zhang, O. Onireti, P. Xiao, M. A. Imran, and R. Tafazolli, "Mixed-numerology signals transmission and interference cancellation for radio access network slicing," *IEEE Trans. Wireless Commun.*, vol. 19, no. 8, pp. 5132–5147, Apr. 2020.

[7] L. Marijanović, S. Schwarz, and M. Rupp, "Intercarrier interference of multiple access UFMC with flexible subcarrier spacings," in *Proc. Eur. Signal Process. Conf.*, Oct. 2017, pp. 888–892.

[8] L. Marijanovic, S. Schwarz, and M. Rupp, "A novel optimization method for resource allocation based on mixed numerology," in *Proc. ICC*, May 2019, pp. 1–6.

[9] F. Lotfi and O. Semiari, "Performance analysis and optimization of uplink cellular networks with flexible frame structure," in *Proc. VTC (Spring)*, Apr. 2021, pp. 1–5.

[10] J. Mao, L. Zhang, P. Xiao, and K. Nikitopoulos, "Interference analysis and power allocation in the presence of mixed numerologies," *IEEE Trans. Wireless Commun.*, vol. 19, no. 8, pp. 5188–5203, May 2020.

[11] A. B. Kihero, M. S. J. Solaija, and H. Arslan, "Inter-numerology interference for beyond 5G," *IEEE Access*, vol. 7, pp. 146 512–146 523, 2019.

[12] C. Johnson, *5G New Radio in Bullets*, 1st ed., 2019.

[13] A. J. Goldsmith, *Wireless Communications*, 2nd ed. Cambridge Univ. Press, 2005.

[14] W. C. Jakes, *Microwave Mobile Communications*. IEEE Press, 1974.

[15] Y. Li and L. J. Cimini, "Bounds on the interchannel interference of OFDM in time-varying impairments," *IEEE Trans. Commun.*, vol. 49, no. 3, pp. 401–404, Mar. 2001.

[16] "Study on channel model for frequencies from 0.5 to 100 GHz (release 16)," 3rd Generation Partnership Project (3GPP), Tech. Rep. 38.901 (v16.1.0), 2020.